ELSEVIER

Polymer 41 (2000) 7855–7864

polymer

Primary and secondary crystallization processes of poly(ϵ-caprolactone)/styrene oligomer blends investigated by pulsed NMR

T. Ikehara*, T. Nishi

Department of Applied Physics, School of Engineering, The University of Tokyo, 7-3-1, Hongo, Bunkyo-ku, Tokyo 113-8656, Japan

Received 14 September 1999; received in revised form 24 December 1999; accepted 29 January 2000

Abstract

The crystallization process of poly(ϵ-caprolactone)/oligostyrene (PCL/OS) blends was analyzed by measuring the spin–spin relaxation time T_2 by pulsed NMR. We examined: (i) the temporal changes of T_2 and the fractional amount f of the crystalline, amorphous, and intermediate components in the primary and secondary crystallization processes; and (ii) the dependence of the behavior on the crystallization temperature T_c and the OS content ϕ_{OS}. The decrease of T_2 of the intermediate and amorphous components with increasing ϕ_{OS} indicated that OS rejected during crystallization is mixed with the residual amorphous PCL as well as trapped in the interface between a lamellar crystal and an amorphous layer. The fraction of the crystal, which is the crystallinity based on the number of protons, decreased with increasing T_c. This is ascribed to the polydispersity of PCL. The values of f of the crystalline and amorphous components depended less on T_c and ϕ_{OS} after the secondary crystallization proceeded than at the end of the primary process. This indicates that the secondary crystallization has the effect of annealing. The fraction of the interface can be an index of regularity of the lamellar structure. Its change implied which process of lamellar thickening, lamella generation, and the rejection of OS was dominant in the secondary crystallization. We also discussed which region OS was rejected into. The changes of f of the three components in the secondary process showed extreme values at $\phi_{OS} \simeq 5\%$. To discuss this behavior, we proposed two possibilities, namely the influence of the morphology of the spherulites and local phase separation during crystallization.

Keywords: Crystallization; Polymer blends; Pulsed NMR

1. Introduction

Pulsed NMR, among various methods to investigate the crystallization process of polymers [1–3] and polymer blends [4,5], is not widely employed so far in spite of its advantages. It is able to obtain information on heterogeneous phases such as molecular mobility and the fractional amounts in the system. When the crystallization process is slow enough compared with the rate of one measurement routine, it is possible to investigate in situ crystallization process of crystalline polymers, which have intrinsic heterogeneity inside, from a melt in the temperature-controlled NMR probe. The spin–spin relaxation time T_2 is mostly employed to obtain the information on a system where small domains of low molecular mobility are dispersed since spin diffusion often loses the information in the measurements of the spin–lattice relaxation time T_1 and the spin–lattice relaxation time in the rotating frame $T_{1\rho}$.

Melt crystallized polymers exhibit the morphology of lamella–stack crystals, in which immobile crystals, mobile amorphous, and intermediate interfacial zones coexist. Pulsed NMR is able to analyze the behavior of the three states individually by decomposing relaxation curves. One of the features of pulsed NMR is the ability to obtain the information relatively easily on the interface [6–12]. A detailed discussion of the crystallization process of poly(ϵ-caprolactone) (PCL) analyzed by pulsed NMR is found elsewhere [12]. The possibility of detection of the pre-ordering state in the early stage of the crystallization process was discussed for PCL blended with oligostyrene (OS) [13].

Crystallization of polymers can be divided into two processes, namely primary and secondary crystallization. Spherulites grow outward until they collide with neighbors in the primary process, while lamellar thickening, crystallization of interlamellar amorphous chains, and the changes

* Corresponding author. Tel.: +81-3-5841-6822; fax: +81-3-5841-6822.

E-mail address: ike@west.t.u-tokyo.ac.jp (T. Ikehara).

0032-3861/00/$ - see front matter
PII: S0032-3861(00)00134-8

Table 1
The characteristics of the samples in this work. Here, M_n is the number average molecular weight, M_w is the weight average molecular weight, T_m^0 is the equilibrium melting temperature, and T_g is the glass transition temperature

Sample	Source	M_n	M_w	T_m^0 (K)	T_g (K)
PCL	Scientific Polymer Products	9300	14 600	333	213
OS	Tohso	836	946	–	288

of lamellar structure occur in the secondary process. The slow rate and the required long period for measurement of the secondary process make the detailed studies still insufficient in spite of its importance.

An amorphous polymer acts as impurities in crystalline/amorphous polymer blends. The mixed impurities cause melting temperature depression, changes in morphology, and the decrease of the spherulite growth rate. The amorphous polymer is rejected from the crystals into interlamellar, interfibrillar, and interspherulitic regions [14].

There are works on the crystallization process of PCL/OS blends as a crystalline/amorphous blend system by optical microscopy [15] and time-resolved X-ray diffraction [16,17]. They mainly focused on the changes of the structures during crystallization. On the other hand, pulsed NMR analyzes the process from the view point of molecular mobility. It also enables us to examine the secondary crystallization process when the measurement is continued for a sufficiently long time after the completion of the primary process. Local phase separation during crystallization was also discussed in the works by optical microscopy [15] and X-ray diffraction [18].

The aim of the present paper is to analyze the crystallization process of crystalline/amorphous polymer blends, PCL/OS, by measuring T_2 by pulsed NMR. We examined the temporal changes of the crystalline, amorphous, and intermediate components in the crystallization process and the dependence of the behavior on the crystallization temperature and the amorphous polymer content. We also report the behavior in the primary and secondary crystallization process, the relation with the morphology of spherulites, and the possibility of local phase separation.

2. Experimental

The characteristics of the polymers are displayed in Table 1. The equilibrium melting temperatures of the blends determined by the Hoffman–Weeks plot [19] are shown in Table 2. The phase diagram of the blends is shown in Fig. 1 along with the melting point depression curve. Since the depression was small, we used temperature itself for displaying the results of temperature dependence instead of the degree of supercooling, which is usually used for analyzing data.

Table 2
Equilibrium melting temperature obtained by the Hoffman–Weeks plot

OS content (%)	T_m^0 (K)
0	332.7
10	332.6
20	332.2
30	331.4

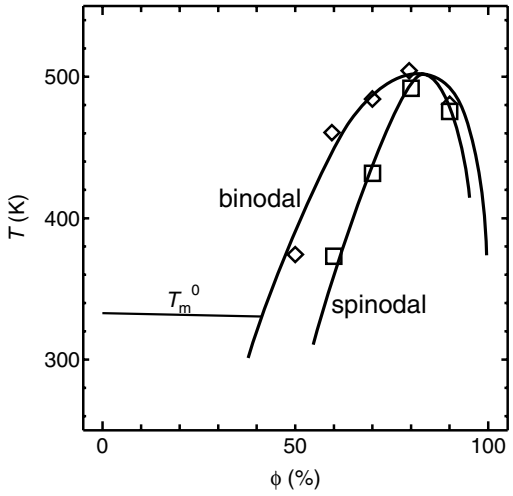

Fig. 1. The phase diagram of the PCL/OS blends showing binodal and spinodal points. The lines are the guides for the eye. It also shows the melting point depression line.

A blend in an NMR sample tube was melted above the melting point of PCL for more than one hour, then transferred into the NMR probe head whose temperature was kept at an experimental crystallization temperature. This moment is the time origin of the crystallization time t. Then, T_2 signals were acquired at desired t with solid echo and CPMG pulse sequences. The signals were analyzed by the nonlinear least-squares fitting method and we obtained the values of T_2 and the fractional amounts of the components. The crystallization temperature T_c, the OS content ϕ_{OS}, and the sample codes are displayed in Table 3. The crystallization process was too slow to obtain satisfactory data for high OS content samples at high T_c. Optical microscopy showed that no phase separation took place under the

Table 3
The experimental conditions of the crystallization temperature T_c, the blend composition ϕ_{OS} and the sample codes. The experiments were carried out under the conditions marked by circles, and not performed under the conditions marked by crosses

Sample code	ϕ_{OS} (%)	T_c (K)			
		308	312	315	318
OS0	0	○	○	○	○
OS1	1	○	○	○	○
OS5	5	○	○	○	×
OS10	10	○	○	○	×
OS20	20	○	○	○	×
OS30	30	○	○	×	×

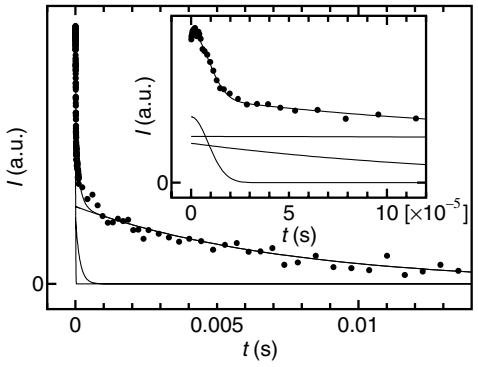

Fig. 2. An example of a transverse relaxation signal decomposed into three components. $\phi_{OS} = 10\%$, $T_c = 312$ K, and $t = 3.2 \times 10^3$ s.

present conditions. The other details of the experiments are described elsewhere [13].

We measured T_2 of the samples crystallized for three days ($\equiv t_t$) and employed these data as the terminal value of the secondary crystallization process though crystallinity was still changing gradually at this point.

3. Results

Fig. 2 is an example of a transverse relaxation signal decomposed into three components (one Gaussian and two exponential curves). The components of short, intermediate, and long T_2 were assigned to the crystalline, interfacial, and amorphous components, respectively as described in the works on crystalline polymers [6–12]. OS in the blend samples is rejected from the crystals during the crystallization process. It is mixed with amorphous PCL or trapped in the interfaces as discussed later. The components with the longest and intermediate T_2 of the blend samples therefore contain the contributions of rejected OS. In Fig. 3, T_2 of pure OS is plotted against temperature. Molecular mobility of OS is lower than that of the intermediate and amorphous components and is close to that of the crystalline phase under the conditions of the present paper. However, when OS is mixed with PCL in amorphous regions and interfaces on the molecular level, the signals of PCL and OS were not

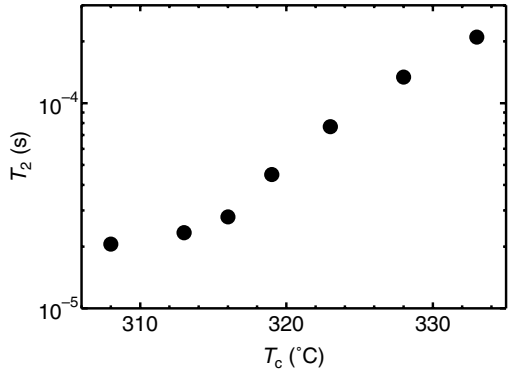

Fig. 3. Temperature dependence of T_2 of oligostyrene.

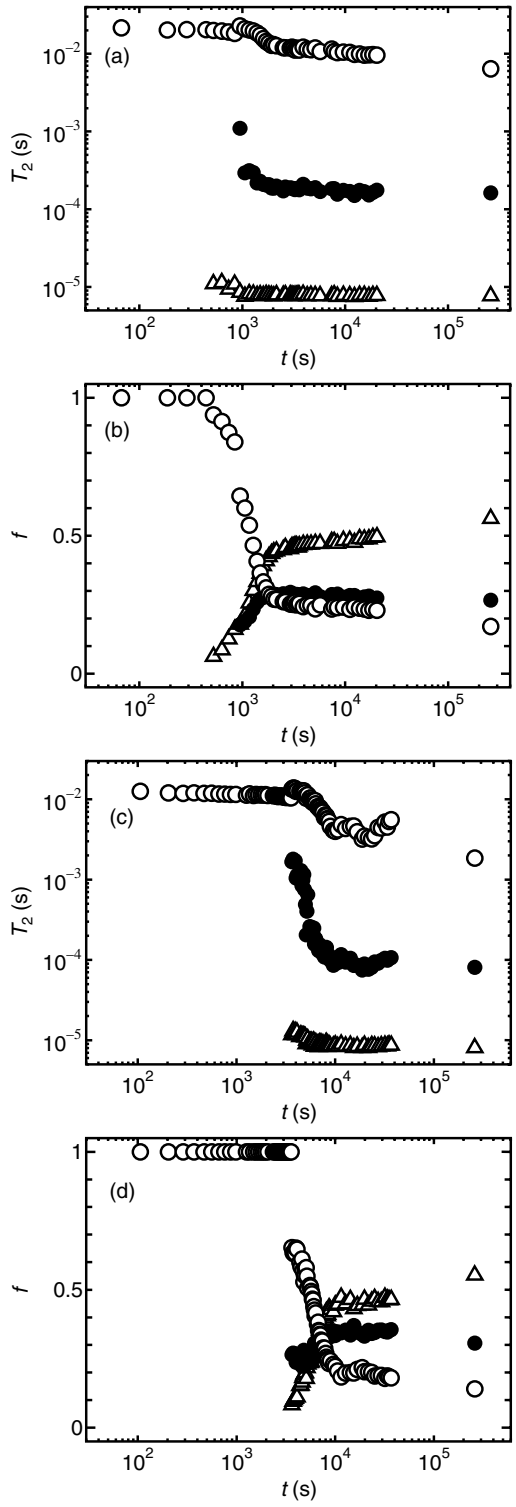

Fig. 4. Examples of the temporal changes of T_2 and f: (a) T_2 and (b) f of pure PCL crystallized at 315 K; (c) T_2; and (d) f of the $\phi_{OS} = 30\%$ blend crystallized at 312 K. ○ amorphous; △ crystalline; and ● intermediate components.

decomposed and were fitted with one component in the signals of pulsed NMR.

Examples of the temporal change of T_2 and the fraction f are shown in Fig. 4 for OS0 crystallized at 315 K and OS30

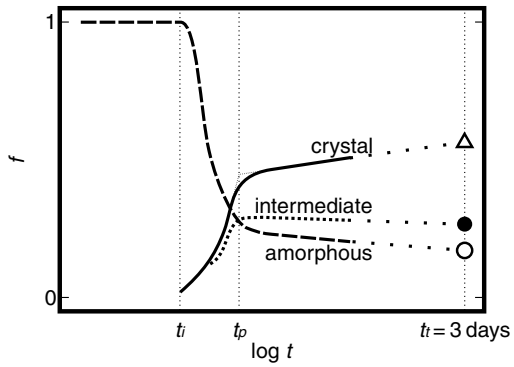

Fig. 5. A schematic figure of the temporal change of the fractional amounts of the components measured by pulsed NMR and notations of the time of the boundary in the process: t_i is the time when the crystalline component emerges, t_p is the time of the boundary of the primary and secondary crystallization process, and t_t is the terminal crystallization time (three days).

crystallized at 312 K. The transverse relaxation curve of the amorphous melt exhibited only one exponential component before the onset of crystallization. The signals have contributions both from PCL and OS melt for $\phi_{OS} > 0$. After the induction period, the crystalline component of OS0 emerged at $t_i \simeq 5 \times 10^2$ s. The slope of the crystalline component changed at $t_p \simeq 2 \times 10^3$ s; this is the boundary of the primary and secondary crystallization processes. The boundaries of t are schematically shown in Fig. 5. The fraction of the crystal f_c and the amorphous component f_a rapidly increased and decreased in the primary process, respectively. In the secondary process, f_c and the fraction of the intermediate component f_i increased gradually, while f_a decreased. The values of T_2 of all the components decreased slowly. The concave shape of f_i of OS30 in the early stage of crystallization is discussed elsewhere [13].

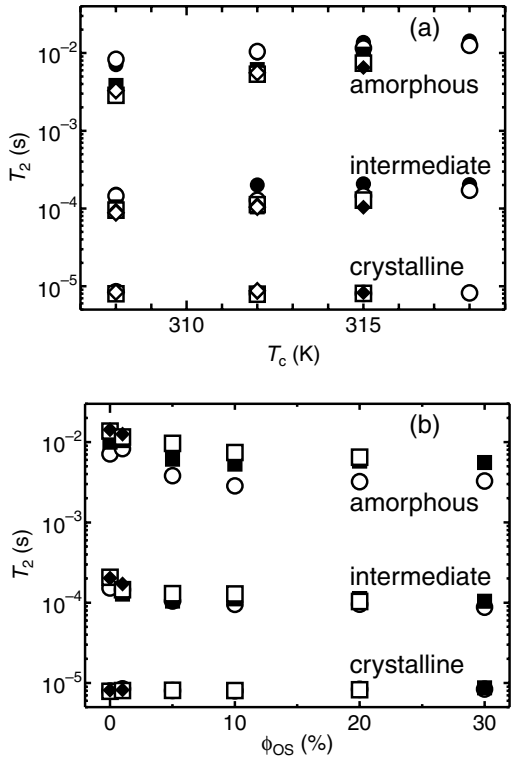

Fig. 6. Dependence of T_2 on (a) T_c and (b) ϕ_{OS} at the end of the primary crystallization process. (a) ● $\phi_{OS} = 0\%$, ○ 1%, ■ 5%, □ 10%, ◆ 20%, and ◇ 30%. (b) ○ $T_c = 308$ K, ■ 312 K, □ 315 K, and ◆ 318 K.

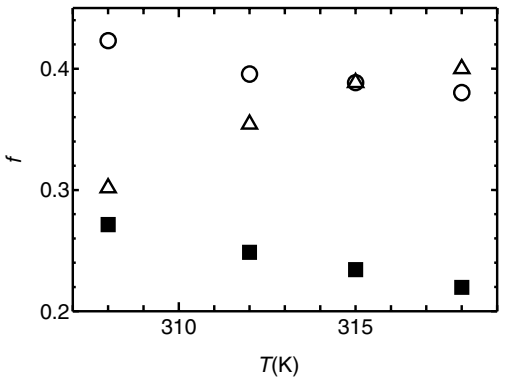

Fig. 7. Crystallization temperature dependence of the fractional amount of each component: ○ crystal, ■ intermediate, and △ amorphous, of a $\phi_{OS} = 5\%$ sample at t_p.

Fig. 6 shows the dependence of T_2 on T_c and ϕ_{OS}. The values of T_2 of the intermediate and amorphous components increased with T_c and decreased with increasing ϕ_{OS}. The dependence of f for OS5 on T_c at t_p is displayed in Fig. 7. This figure shows that f_c and f_i decrease with increasing T_c while f_a increases.

Figs. 8–10 display in detail the dependence of f on T_c and ϕ_{OS}. The values both at t_p and t_t are shown in Figs. 8 and 9. The data only at t_p are shown for the intermediate component since the changes of f_i were not large enough between t_p and t_t.

Fig. 11 shows the polarized optical micrographs of the spherulites of the samples. As ϕ_{OS} increased, spherulites gradually showed fibrillar structures for $\phi_{OS} \gtrsim 5\%$. This indicates that the impurities started to be rejected into the interfibrillar regions at 5%.

4. Discussion

4.1. Changes of T_2

In the primary process, T_2 of the three components decreased as shown in Fig. 4. These results indicate that the progress of crystallization suppresses molecular mobility in all the three components. The suppression of mobility of the crystalline and intermediate components with time is attributed to the perfection of the crystalline structure, i.e. crystals with fewer defects inside have lower mobility and they also suppress the mobility in the connected interfaces. The situation of the amorphous phase is different. It consists

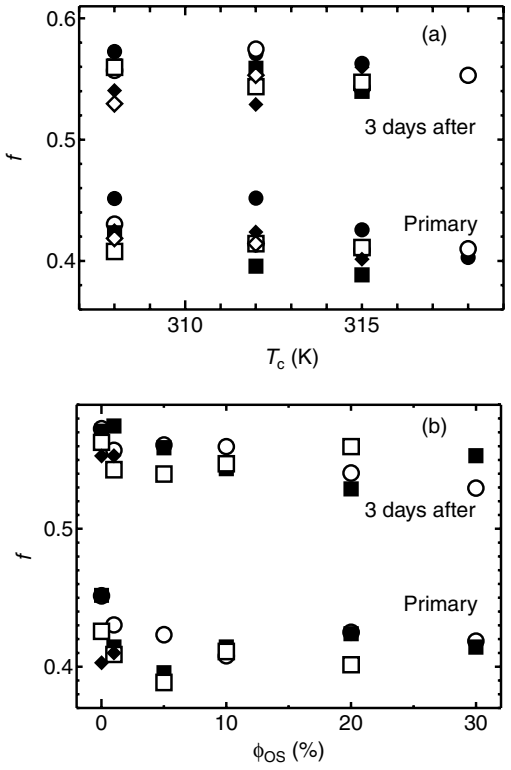

Fig. 8. (a) Crystallization temperature and (b) OS content dependence of the fraction of the crystalline component in transverse relaxation signals at t_p and t_t. The symbols are identical to those in Fig. 6.

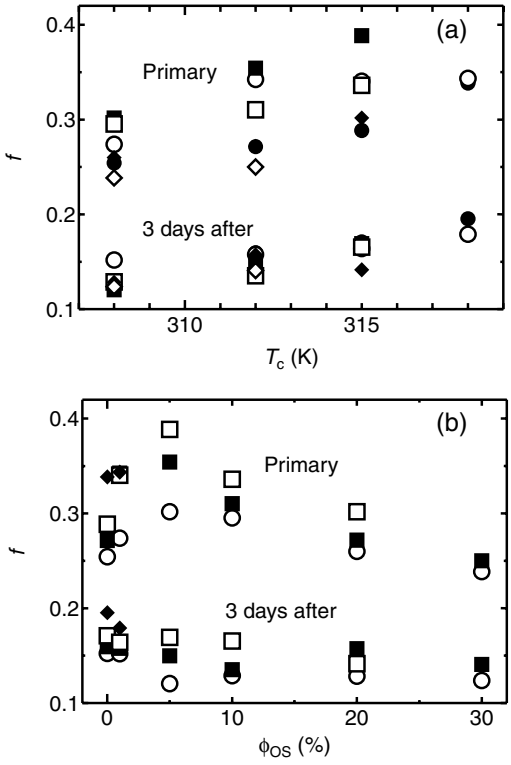

Fig. 9. (a) Crystallization temperature and (b) OS content dependence of the fraction of the amorphous component in transverse relaxation both at t_p and t_t. The symbols are identical to those in Fig. 6.

of the relatively mobile amorphous melt outside the spherulites and the relatively immobile interlamellar amorphous chains constrained by lamellae. The difference in T_2 of the amorphous melt and the interlamellar amorphous chains is too small for pulsed NMR to decompose their signals. The decrease of T_2 of the amorphous phase in the primary process is a consequence of the decrease of the amount of the amorphous melt and the increase of that of the interlamellar amorphous chains. The gradual decrease of T_2 of the interfacial and amorphous components in the secondary process suggests some structural changes in these regions. The increase of f_c and the decrease of f_a and f_i in the secondary process is the consequence of the growth of the crystals which incorporate surrounding interfaces and amorphous chains. The value of T_2 for the crystalline component, on the other hand, is almost constant as discussed with Eq. (2) below.

The change of T_2 can be understood based on the theory of the line shape [20]. The magnetization $M(t)$ in the spin–spin relaxation process is described by

$$M(t) = M_0 \exp[-\sigma_0^2 \tau_c^2 \{\exp(-t/\tau_c) + t/\tau_c - 1\}] \quad (1)$$

where M_0 is the initial magnetization, σ_0^2 is the second moment of the resonance line of the rigid lattice, and τ_c is the correlation time of the fluctuating local field arising from surrounding spins. When mobility is small, i.e. $\sigma_0 \tau_c \gg 1$, as

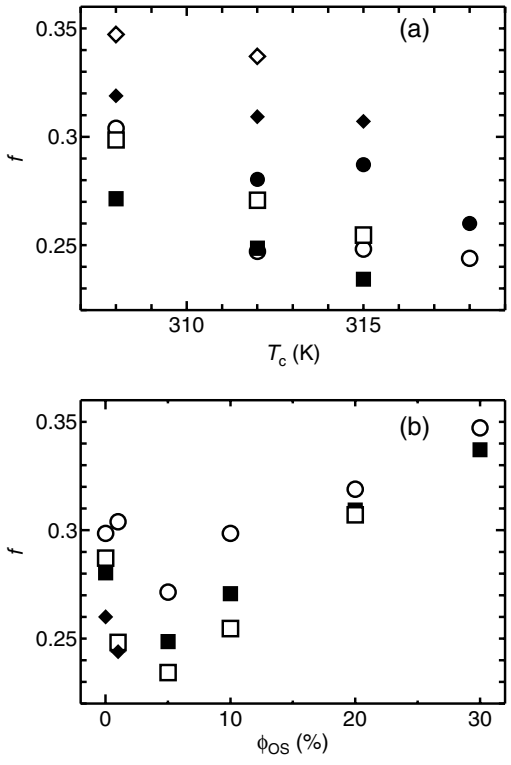

Fig. 10. (a) Crystallization temperature and (b) OS content dependence of the fraction of the intermediate component in transverse relaxation signals at t_p. The symbols are identical to those in Fig. 6.

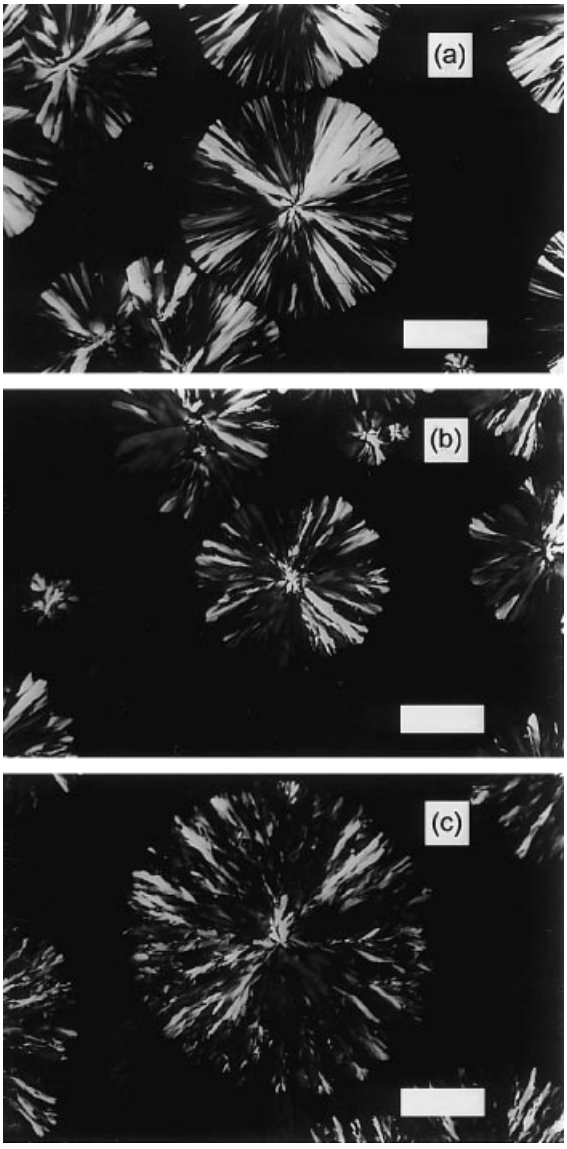

Fig. 11. Polarized micrographs of spherulites of PCL blended with styrene oligomer. (a) $\phi_{OS} = 0\%$, $t = 20$ min, (b) $\phi_{OS} = 5\%$, $t = 21$ min. (c) $\phi_{OS} = 10\%$, $t = 43$ min. Bar = 100 μm.

in crystals, Eq. (1) reduces to

$$M(t) = M_0 \exp[-(t/T_2)^2/2] \quad (2)$$

where $T_2 = \sigma_0^{-1}$. The value of T_2 is independent of molecular mobility at this limit. When mobility is large, i.e. $\sigma_0 \tau_c \ll 1$, it is expressed by

$$M(t) = M_0 \exp(-t/T_2) \quad (3)$$

where $T_2 = \sigma_0^{-2} \tau_c^{-1}$. Eq. (2) describes the relaxation of the crystalline phase and Eq. (3) describes that of the intermediate and amorphous components.

The values of T_2 of the intermediate and amorphous components increase with T_c as shown in Fig. 6. This is explained by decreased τ_c by thermal motion. On the other hand, T_2 of the crystalline component is almost constant since the change of τ_c affects T_2 only slightly in a solid system.

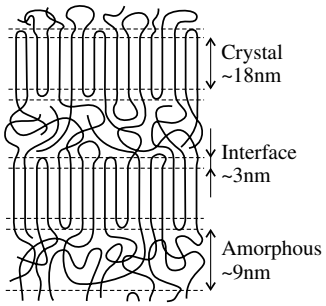

Fig. 12. Schematic figure of lamella crystals showing crystalline, interfacial, and amorphous zones.

The decrease of T_2 of the intermediate and amorphous components with increasing ϕ_{OS} (Fig. 6b) is the evidence that the OS rejected from crystals is mixed with PCL on the molecular level in amorphous regions and in interfaces for the following reasons. First, the value of T_2 is determined by the molecular mobility on a local spatial scale, which is usually less than of the order of 1 nm. Second, the mobility of pure OS is lower than that of amorphous PCL in the present experimental temperature range (Fig. 3). The decrease of T_2 in Fig. 6b shows the existence of the immobile protons of OS close to the mobile protons of PCL in amorphous and interfacial regions. The value of T_2 of the crystal, on the other hand, is independent of ϕ_{OS} though mixed OS may make the crystalline structure less perfect and decrease τ_c. This is because the situation in crystals is in the immobile limit as explained above by Eq. (2).

4.2. Changes of f

The structure of lamellar crystals is schematically shown in Fig. 12. In the work on pure PCL by pulsed NMR [11], the thickness of a crystal, an interface, and an amorphous layer of PCL was estimated to be 18, 3 and 9 nm, respectively, by assuming an ideal two-dimensional (2D) lamellar structure. Since two interfacial regions are on both sides of a lamellar crystal, the value of f_i is twice what is estimated from the thickness. This estimation is also applicable to the present data of pure PCL and gave almost the same values. For example, they were 18, 5 and 9 nm, respectively, for OS0 at $T_c = 315$ K.

The value of f_c is the crystallinity based on the number of protons. It is easily converted into weight crystallinity $f_c^{(w)}$ with the ratios of the number of the protons in the repeating unit to its molecular weight of the constituent polymers. In the present system, the two crystallinities are almost the same ($f_c^{(w)} = 0.96 f_c$ at $\phi_{OS} = 30\%$ and $f_c^{(w)} = f_c$ at 0%).

The increase of f_c and the decrease of f_a with increasing T_c in Fig. 7 is ascribed to the polydispersity of PCL [21]. The molecules with lower molecular weight have less chance to crystallize at higher T_c; the amount of the crystallizable PCL decreases with increasing T_c. The decrease of f_i is the

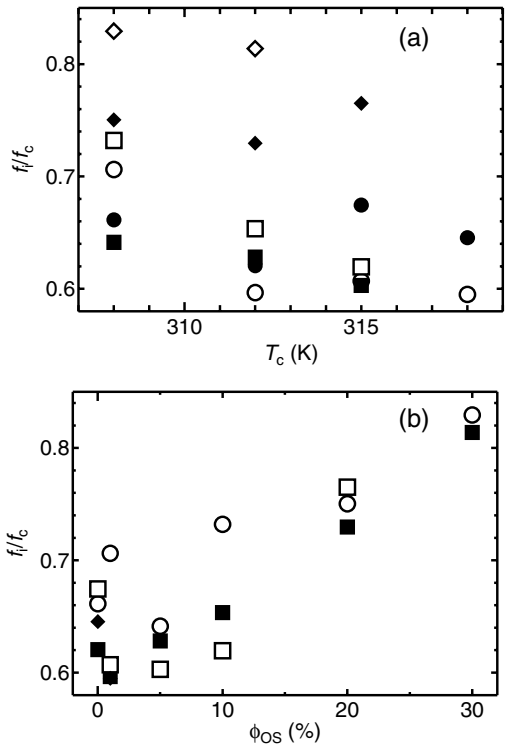

Fig. 13. Plots of the ratio of f_i to f_c against (a) T_c and (b) ϕ_{OS} at t_p. The symbols are identical to those in Fig. 6.

consequence of the more regular lamella–stack structure created at higher T_c through a slower crystallization rate. The fraction of the interface can be an index of regularity of the lamellar structure since it is a defect that does not exist in an ideal crystal.

The details of the behavior of f are displayed in Figs. 8–10. First, we look at the behavior of the crystal. Fig. 8 shows less dependence of f_c on T_c and ϕ_{OS} at t_t than at t_p. This implies that the secondary crystallization process has the effect of annealing. It diminished the differences in the crystallization conditions. The annealing effect appears in the amorphous component as well (Fig. 9). It also shows less dependence on T_c and ϕ_{OS} at t_t than at t_p. The maximum at $\phi_{OS} = 5\%$ at t_p is discussed later.

Next, we discuss the behavior of f_i based on the relation with the regularity of the lamellar structure mentioned above in the discussion of Fig. 7. Fig. 10 shows that lower T_c and higher ϕ_{OS} results in a large value of f_i. On the other hand, the change of f_c must also be considered in discussions of f_i since interfacial layers always accompany a crystal; the amount of interfaces is dependent on that of crystals as well.

Figs. 7, 8 and 10 show both f_c and f_i decreases with increasing T_c. These figures do not clearly show whether f_i really decreases or the decrease of f_i is a consequence of the decrease of f_c. When discussing the behavior of the interface, we have to consider the ratio f_i/f_c rather than f_c and f_i, respectively to clarify the change of the interface. Fig. 13a shows the plot of f_i/f_c against T_c at t_p. It enables us to confirm the decrease of f_i with increasing T_c. It indicates that the lamellar structure crystallized at higher temperature is more regular when the relation between the amount of the interface and regularity of the lamellar structure is considered as mentioned above.

The value of f_c was almost constant and f_i increased with ϕ_{OS} for $\phi_{OS} \gtrsim 5\%$ at t_p as shown in Figs. 8 and 10. The plot of f_i/f_c against ϕ_{OS} at t_p is shown in Fig. 13b, which indicates the increase with ϕ_{OS}. When ϕ_{OS} dependence of f_i/f_c is discussed, the contributions of OS in the interfaces must be taken into account. There are two reasons considered for the increase of f_i/f_c. One is the low regularity of the lamellar structure because of the existence of the impurities. The other is the contribution of rejected OS coexisting with PCL in interfaces on the molecular scale as discussed with the T_2 data (Fig. 6b). The present data do not show which factor is dominant in the PCL/OS systems. It requires more investigation to clarify the influences of ϕ_{OS} on f_i.

4.3. Secondary crystallization

To examine what happens in the secondary crystallization process, the ratio of f at t_t to that at t_p (f_t/f_p) was plotted against ϕ_{OS} in Fig. 14. The values of f_t/f_p of the crystalline and intermediate components have maxima at $\phi_{OS} \simeq 5\%$ and the amorphous component has a minimum at 5%.

The secondary crystallization is an ordering process in which the structures of melt crystallized polymers change to be closer to the ideal crystal with no defect such as interfaces or the lamellar stack structures. In this process: (i) lamellar thickening; (ii) lamella generation (crystallization in the interlamellar amorphous zones); and (iii) rejection of OS from the regions of the growing crystals occur. As indicated by Fig. 14a and b, f_c increases ($f_t/f_p > 1$) and f_a decreases ($f_t/f_p < 1$) in the secondary process. The change of f_i varies according to the above three cases. In case (i), where existing crystals grow incorporating surrounding amorphous chains and interfaces, f_i decreases because of the effect of incorporation into the growing crystals. In case (ii), f_i must increase since new lamellar crystals and accompanying interfaces appear. In case (iii), part of the rejected OS must be trapped in interfaces as in the primary crystallization discussed with Fig. 6b. This factor increases f_i. This process occurs both in case (i) and (ii). The situations of cases (i)–(iii) are schematically illustrated in Fig. 15. The increase or decrease of f_i indicates which case is in progress in the secondary crystallization process.

The intermediate component shows $f_t/f_p > 1$ for $1 \lesssim \phi_{OS} \lesssim 20$ and $f_t/f_p < 1$ otherwise as indicated in Fig. 14c. Since the plot shape is similar to that of f_c (Fig. 14a), the increase or decrease of f_i must be related to the amount of the crystals created in the secondary process. Cases (ii) and (iii) explain the change of the intermediate component since f_c and f_i show the same plot shape in these cases. On the contrary, f_t/f_p for the crystal and interface would show opposite plot shapes in case (i). However, lamellar thickening plays an important role at least in the regions where $f_t/f_p < 1$

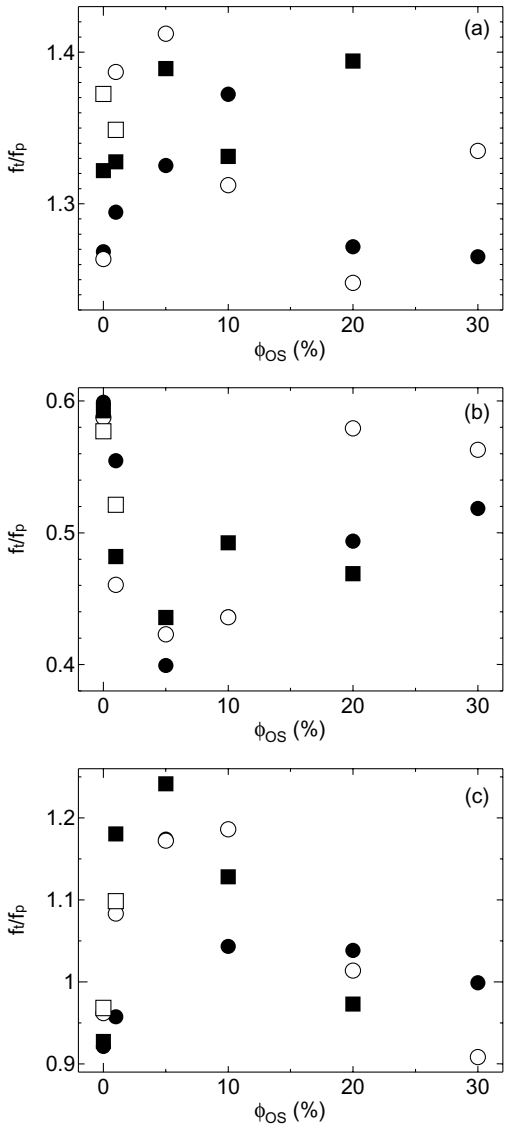

Fig. 14. Styrene oligomer content dependence of the ratio of the fraction of each component at t_t to that at t_p: (a) crystalline; (b) amorphous; and (c) intermediate component. The symbols are identical to those in Fig. 6b.

for the interface. PCL lamellae are reported to thicken after about 10^3 s of crystallization time according to the study of the melting point [22]. On the other hand, X-ray scattering experiments showed that lamellae in PCL/PS do not thicken [16] and that the long period is almost constant [17] during the shorter crystallization periods of around 10^3 s.

The plot shape of the crystal in Fig. 14a is also similar to that of the amorphous component at t_p in Fig. 9b. This indicates that the amount of the crystal increases more in the secondary process when a larger amount of amorphous chains is still left at t_p.

4.4. Rejection of impurities

According to Fig. 11, fibrillar spherulites become observable by optical microscopy at $\phi_{OS} \simeq 5\%$. During crystallization OS is rejected from crystals into three possible areas, namely interlamellar, interfibrillar, and interspherulitic zones [14]. Since optical micrography showed that spherulites of the blends fill the whole volume, the interspherulitic regions are ruled out as the destination of rejected OS. It is mainly interlamellar regions when the fibrillar structure is unclear ($\phi_{OS} \lesssim 5\%$). For $\phi_{OS} \gtrsim 5\%$, it must be rejected into both interlamellar and interfibrillar zones.

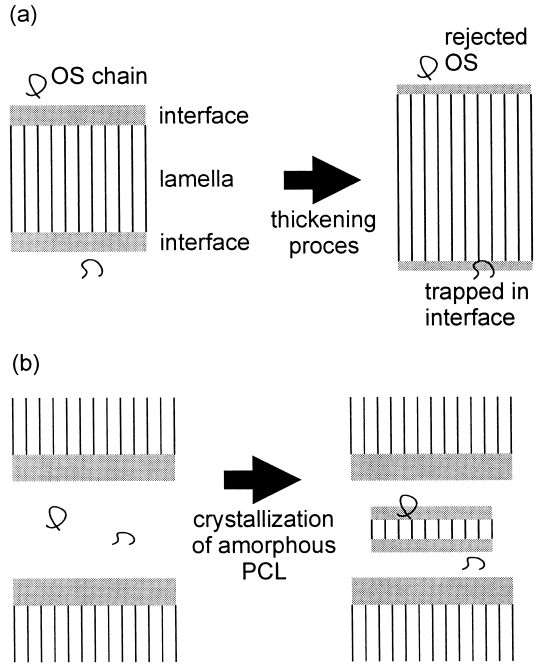

Fig. 15. (a) Schematic figure of lamellar thickening process in which existing lamellae grow incorporating surrounding interfaces and amorphous chains. (b) Schematic figure of the crystallization in an interlamellar amorphous zone. The new lamella appears along with the interfaces.

The PCL/OS blends with the present molecular weights undergo phase separation at $\phi_{OS} \simeq 40\%$ (Fig. 1). It may occur in the amorphous regions since the rejection of OS increases ϕ_{OS}. The values of ϕ_{OS} of the two phases after phase separation are about 40% and almost 100% according to the phase diagram.

The following two hypotheses are proposed here. One is that the change of the behavior at $\phi_{OS} = 5\%$ in Fig. 14 is ascribed to the change of morphology of spherulites. It explains the ϕ_{OS} dependence of f_c at t_p (Fig. 8b). For $\phi_{OS} \lesssim 5\%$, rejected OS increases the local value of ϕ_{OS} around growing crystals and lessens the amount of the crystals produced in the primary process. For $\phi_{OS} \gtrsim 5\%$, OS is additionally rejected into the interfibrillar zones. This effect slows down the increase of local ϕ_{OS}; the value of f_c at t_p is affected little by the blend composition. This relationship between morphology and the results of NMR, however, must be investigated farther to confirm its validity.

The second hypothesis is that ϕ_{OS} increased by the rejection of OS induces local phase separation in interlamellar amorphous regions. It can explain the change at 5% in Figs.

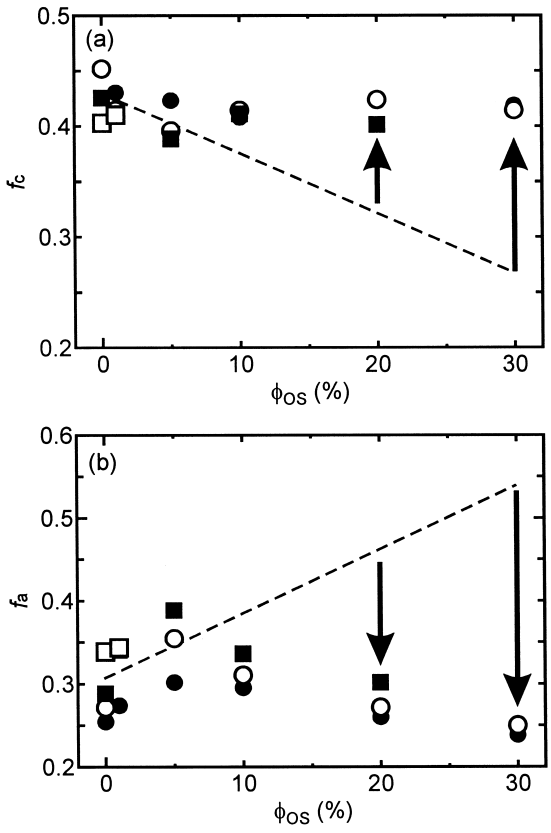

Fig. 16. Schematic illustration that explains the changes of (a) f_c and (b) f_a at t_p induced by phase separation.

8b and 9b as follows: the composition of the OS-rich phase, which emerges with phase separation, is nearly OS 100%. Its T_2 is close to that of the crystalline state (Fig. 3). The NMR signal from the OS-rich phase is therefore superposed on the crystalline component since NMR in our experiments does not have enough resolution to decompose the two phases. As schematically indicated in Fig. 16 f_c increases and f_a decreases approximately by the amount of the emerging OS-rich phase.

The condition that phase separation takes place is expressed by

$$\phi_{OS}^{(res)} = \phi_{OS}/(1-\theta) > \phi_b \quad (4)$$

where $\phi_{OS}^{(res)}$ is the local blend composition in the residual amorphous regions after crystallization, θ is weight crystallinity ($0 < \theta < 1$), and ϕ_b is the binodal composition ($\simeq$40%) shown in the phase diagram. The value of θ is calculated from the value of the dashed line in Fig. 16a, which is the crystallinity based on the number of protons. The condition of Eq. (4) is met only for $\phi_{OS} \gtrsim 30\%$ with the values of ϕ_{OS}, θ and ϕ_b in the present experiments. The calculated value of $\phi_{OS}^{(res)}$, however, is an average in the whole sample. There is a possibility that the local value of $\phi_{OS}^{(res)}$ around lamellae is different and that phase separation really takes place on a microscopic scale. This hypothesis also requires more investigation.

5. Conclusions

The crystallization process of PCL/OS blends was investigated by measuring the transverse relaxation by pulsed NMR. The decrease of T_2 of the intermediate and amorphous components with increasing ϕ_{OS} indicated that OS is rejected into the residual amorphous PCL and the interfaces during crystallization. The decrease of f_c with increasing T_c is ascribed to the polydispersity of PCL. The values of f_c and f_a depended less on T_c and ϕ_{OS} after the secondary crystallization proceeded than at the end of the primary process. This indicates that the secondary crystallization has the effect of annealing. The value of f_i can be an index of regularity of the lamellar structure. Its change implied which process of lamellar thickening, lamella generation, and the rejection of OS was dominant in the secondary crystallization. We also discussed which region OS was rejected into. The changes of f in the secondary process showed extreme values at $\phi_{OS} \simeq 5\%$. We proposed two hypotheses to discuss this behavior. One is the influence of the morphology of the spherulites. The structural change at 5% into the fibrillar spherulites and the additional exclusion of the impurities into interfibrillar zones may explain it. The other is the possibility of local phase separation during crystallization. The increased value of ϕ_{OS} in the interlamellar regions induces phase separation on a small scale. It produces a phase whose ϕ_{OS} is almost 100%. The values of f_c and f_a change by the amount of it.

References

[1] Mandelkern L. Crystallization of polymers. New York: McGraw-Hill, 1964.
[2] Wunderlich B. Macromolecular physics, vol. 2. New York: Academic Press, 1980.
[3] Fava RA, editor. Method of experimental physics Polymers part B, crystal structure and morphology, vol. 16. New York: Academic Press, 1980.
[4] Paul DR, Barlow JW. In: Klempner D, Frisch KC, editors. Polymer alloys, vol. II. New York: Plenum Press, 1980.
[5] Utracki LA. Polymer alloys and blends. Munich/Vienna/New York: Hanser, 1989.
[6] Fujimoto K, Nishi T, Kado R. Polym J 1972;3:448.
[7] Kitamaru R, Horii F, Hyon S-H. J Polym Sci: Polym Phys Ed 1977;15:821.
[8] McBrierty VJ, Douglass DC. J Polym Sci: Macromol Rev 1981;16:295.
[9] McBrierty VJ, Douglass DC. Phys Rep 1980;63:63.
[10] Douglass DC, McBrierty VJ, Weber TA. J Chem Phys 1976;64:1533.
[11] Tanaka H, Nishi T. J Appl Phys 1986;59:1488.
[12] Tanaka H, Nishi T. J Chem Phys 1986;85:6197.
[13] Ikehara T, Nishi T. Acta Polym 1995;46:419.
[14] Stein RS, Khambatta FB, Warner FP, Russell T, Escala A, Balizer E. J Polym Sci: Polym Symp 1978;63:313.
[15] Tanaka H, Nishi T. Phys Rev A 1989;39:783.

[16] Li Y, Jungnickel BJ. Polymer 1993;34:9.
[17] Nojima S, Kato K, Ono M, Ashida T. Macromolecules 1992;25:1922.
[18] Nojima S, Satoh K, Ashida T. Macromolecules 1991;24:942.
[19] Hoffman JD, Weeks JJ. J Res Natl Bur Stand 1962;66A:13.
[20] Kubo R, Tomita K. J Phys Soc Jpn 1954;9:888.
[21] Gornick F, Mandelkern L. J Appl Phys 1962;33:907.
[22] Phillips PJ, Rensch GJ. J Polym Sci Part B: Polym Phys 1989; 27:155.